

**Thermal diffusivity of Tungsten ion irradiated
Tungsten-Tantalum alloys as measured by
Transient Grating Spectroscopy**

by

Emilio Ahuactzin-Garcia

Submitted to the Department of Nuclear Science and Engineering
in partial fulfillment of the requirements for the degree of
Bachelor of Science in Nuclear Science and Engineering
at the

MASSACHUSETTS INSTITUTE OF TECHNOLOGY

June 2024

©2024 Emilio Ahuactzin-Garcia. All rights reserved.

The author hereby grants to MIT a nonexclusive, worldwide,
irrevocable, royalty-free license to exercise any and all rights under
copyright, including to reproduce, preserve, distribute and publicly
display copies of the thesis, or release the thesis under an open-access
license.

Author
Emilio Ahuactzin-Garcia
Department of Nuclear Science and Engineering
May 10, 2024

Certified by
Michael Short
Associate Professor of Nuclear Science and Engineering
Thesis Supervisor

Accepted by
Jacopo Buongiorno
Professor of Nuclear Science and Engineering
Undergraduate Chair

Thermal diffusivity of Tungsten ion irradiated Tungsten-Tantalum alloys as measured by Transient Grating Spectroscopy

by

Emilio Ahuactzin-Garcia

Submitted to the Department of Nuclear Science and Engineering
on May 10, 2024 in partial fulfillment of the requirements for the degree of

BACHELOR OF SCIENCE IN NUCLEAR SCIENCE AND ENGINEERING

ABSTRACT

One of the primary remaining challenges in the transition from fusion experimental devices to economically viable fusion power plants is the identification of materials that can survive for years in environments such as the divertor. Tungsten-tantalum alloys have demonstrated improved ductility and resistance to radiation damage compared to the pure tungsten currently used in this role, but at the cost of decreased thermal diffusivity in unirradiated samples. However, it is not the unirradiated properties, but those during and after irradiation that define materials performance in power plant environments. A scarcity remains in relevant data for irradiated plasma facing materials. In this work I implanted pure tungsten, as well as tungsten-tantalum alloys of 3%, 6% and 11% weight concentration of tantalum with 10.26 MeV tungsten ions to damage levels over 1 dpa, representative of four months in a DEMO-type fusion device. Transient grating spectroscopy (TGS), a non-destructive optical technique was used to continuously measure thermal diffusivity during irradiation. I found that the tungsten-tantalum alloys demonstrated a reduced fractional thermal diffusivity drop compared to pure tungsten. Despite the lower initial thermal diffusivity in a W-Ta alloy, this behavior indicates that such alloys would face less significant property changes during operation, and thus allow for more predictability in fusion reactor design.

Thesis supervisor: Michael Short

Title: Associate Professor of Nuclear Science and Engineering

Acknowledgments

I wish to thank Rachel Shulman and the MIT FUSars program for supporting this project. I also thank Samantha Karlson for her help in the irradiation experiments, Mike Short for his help in reviewing this work, and Angus Wylie for his incredible efforts during experimentation. He truly went above and beyond, and this thesis would not be possible without him. I thank the MIT UROP office, Mimi Slaughter, and MathWorks for providing funding for this project.

Contents

Title page	1
Abstract	3
Acknowledgments	5
List of Figures	9
1 Introduction	11
2 Background	13
3 Methods	19
3.1 Experimental method	19
3.2 Analytical Methods	23
4 Results	25
4.1 TGS traces	25
4.2 Observations	25
4.3 Experimental Challenges	26
5 Discussion	33
6 Conclusion	37
A Transmutation and realistic irradiation of Tungsten-Tantalum alloys	39
A.1 Motivation	39
A.2 Methods	40
A.2.1 Grasshopper	41
A.2.2 FISPACT-II	42
A.3 Results	43
A.3.1 Grasshopper	43
A.3.2 FISPACT-II	43
A.4 Conclusions	45

B Data Availability 49

References 51

List of Figures

2.1	Diagram of a TGS setup on an accelerator beamline. Adapted from diagram by Cody Dennett and the MNM Group	18
3.1	W-3%Ta sample	20
3.2	Skew of off-axis ion beam	21
3.3	Sample holder. Red outline shows sample and blue outline shows phosphor alignment chip	22
3.4	dpa and W-ion deposition at various sample depths in 10.26 W^{+5} irradiated W-3%Ta alloy. The shaded region indicates the region measured by the TGS probe	23
3.5	TGS signal fit on pure W, showing the thermal decay and surface acoustic wave response	24
4.1	TGS traces for unirradiated samples	28
4.2	TGS traces for samples at saturation	29
4.3	Evolution of thermal diffusivity of tungsten-tantalum alloys under self-ion irradiation	30
4.4	Comparison of initial thermal diffusivity with thermal diffusivity after saturation (averaged over 0.9-1 dpa)	31
5.1	Comparing the evolution of W thermal diffusivity across studies	34
A.1	Geant4 simulation of 14.1 MeV neutrons interacting with a 28 mm thick tungsten alloy block	42
A.2	Transmutation events at differing depths for tungsten-tantalum alloys	46
A.3	Composition over time for W-Ta alloys under fusion neutron irradiation . .	47

Chapter 1

Introduction

Transitioning to a zero emissions society requires an economical and dispatchable source of electricity. Fusion energy has the potential to fill this role. Advances in high temperature superconductors and high field fusion experiments have raised expectations that the field of fusion research may transition from physics experiments to power plant engineering within this decade [1]. Questions remain surrounding what materials can survive for long periods of time in fusion reactor conditions, and do so without producing long-lived radioactive waste. No region faces a more extreme environment than the divertor, which faces bombardment by 14.1 MeV neutrons, direct contact with the fusion plasma, and heat fluxes of 10 MW/m^2 in steady state operation [2]. The divertor is also expected to receive up to 3 dpa per full power year in a DEMO-type device [3]

Tungsten is the leading candidate material for the divertor due to its high strength and melting point [4]. However, tungsten has drawbacks that will likely prevent the use of pure tungsten in fusion power plants. Tungsten has a high ductile-to-brittle transition temperature, an issue worsened by radiation induced lattice damage, void swelling, and transmutation product clustering [5] [6]. Tantalum has shown promise as an additive, improving material and irradiation properties, but at the cost of degrading thermal properties [4][7] [8]. The high heat flux faced by the divertor makes thermal diffusivity a powerful figure

of merit in assessing candidate materials. Characterizing the thermal diffusivity of various tungsten-tantalum alloy compositions over lifetime irradiation is essential in optimizing material choice. Divertors are expected to last for 2 years, and first wall components for up to 5 in a DEMO-type power plant [9]. While this is a much shorter lifespan than fission reactor materials, significant property changes are expected to occur, and lengthening these lifespans are an essential strategy in ensuring the economic viability of fusion.

A large challenge exists around how candidate materials can be rapidly evaluated and iterated upon. The high fusion neutron flux these materials experience is unique, and difficult to replicate. Existing fission reactor neutron sources are insufficient as the neutron flux is too low to produce representative levels of damage quickly enough, and the neutron energy spectrum is not a good match for fusion neutrons [10]. New methods that allow for accelerated iteration while maintaining and even deepening insights into fusion irradiation effects are needed to characterize materials.

The combination of Transient grating spectroscopy (TGS) with heavy ion irradiation of samples allows for the rapid and detailed analysis of the evolution of materials under irradiation. Heavy ion irradiation, by producing the equivalent of years worth of damage in hours, significantly accelerating the rate at which irradiation effects can be produced and analyzed. The indirect, non-destructive nature of TGS means that this technique can be directly coupled with irradiation, allowing for in-situ measurement of evolving material properties during irradiation. These two techniques further synergize, as heavy ion irradiation produces damage cascades similar to high energy neutrons at depths on the order of $1\mu\text{m}$, matching the tunable measurement depth range of TGS, a non-destructive optical technique that measures thermal diffusivity [11] [12].

In this work the use of in-situ TGS measurements to perform an analysis of the evolution of thermal diffusivity of varying tungsten-tantalum alloys under tungsten ion irradiation is presented. This is presented both as an example of a method for rapid iteration of testing for fusion materials, and steps towards the optimization of W-Ta alloys for divertor applications.

Chapter 2

Background

There are several limitations that preclude the use of pure tungsten in fusion power plants. A high ductile-to-brittle transition temperature (DBTT). and irradiation hardening limit tungsten's use [13]. Under the fast neutron irradiation in a fusion reactor, the DBTT rises due to the formation of gas bubbles from transmutation and lattice defects, among various other types of defects. The production of voids and dislocation loops also serves to reduce the thermal conductivity [5]. During irradiation, tungsten is also transmuted to heavy transition metals, primarily rhenium, osmium, and tantalum. The presence of these elements changes the chemical composition of the material, and can form precipitates that result in embrittlement of the tungsten [6].

Various tungsten alloys have been proposed to alleviate these issues, with tantalum showing particular promise [13]. Simulations have shown that tantalum hinders the formation of rhenium clusters [7]. Tantalum also increases ductility, and under proton irradiation have smaller dislocation loop sizes than pure tungsten [4]. This comes with the trade-off of a reduction of thermal diffusivity in as-manufactured samples [8]. As thermal diffusivity determines whether a material can reject the significant heat loads faced in fusion applications, identifying the evolution of thermal diffusivity of various compositions of tungsten-tantalum alloys under irradiation is needed in order to optimize the benefits of tantalum addition.

To determine this evolution, radiation damage must be produced that is analogous to that produced in a fusion reactor, with various existing techniques. Many shortcomings exist with reactor neutron irradiation. Proton irradiation can allow for the simulation of damage and to rapidly produce relevant amounts of damage [10]. However, proton irradiation can induce activation that can lead to long wait times for allowable handling.

Heavy ion irradiation is an effective alternative, featuring damage rates around an order of magnitude higher than proton irradiation, shortening irradiation times to reach significant damage levels from days to hours [14]. Heavy ion irradiation is an effective simulation of the damage produced by neutrons, producing similar large energy transfers and damage cascades, though only at depths on the order of microns and without the transmutation resulting from neutron irradiation [11][15]. Tungsten ion self irradiation has been used as such a method to probe the irradiated behavior of tungsten-tantalum alloys [16]. The use of self-ion irradiation further allows for the exclusion of potential effects resulting from the ion species itself [17].

A key metric for evaluating the performance of plasma materials is thermal diffusivity. Thermal diffusivity is a measure of the rate of heat transfer, given by

$$\alpha = \frac{k}{\rho c_p} \quad (2.1)$$

where α is the thermal diffusivity, k is the thermal conductivity, ρ is the density, and c_p is the heat capacity. Thermal diffusivity measurements can give vital information about a material's ability to handle and reject heat loads. This is of particular importance for plasma facing materials (PFMs). PFMs must be able to handle heat loads of 10 MW/m^2 in normal operation, and many times more during disruptions. PFMs have energy deposition limits in place in order to prevent erosion, with thermal diffusivity playing a vital part in determining the energy deposition that corresponds to melting conditions. The prevention of erosion has twofold importance. Erosion determines the lifetime of the material, but also

the fusion performance, as the presence of high-Z elements such as tungsten in the fusion plasma greatly raises bremsstrahlung losses in the plasma [18]. Thus, the thermal diffusivity of a plasma facing material is vital in determining its viability in a fusion power plant.

The standard method for thermal diffusivity measurement is the flash method. In this method, one end of a sample is illuminated by a pulse of laser or flashbulb light, and the temperature response is measured on the opposite side of the sample. With this information, the rate of heat transfer, and thus the thermal diffusivity can be determined, as the sharp heating pulse results in temperature changes dependent only on thermal diffusivity. The thermal diffusivity is determined by

$$\alpha = 0.1388 \frac{e^2}{t_{0.5}} \quad (2.2)$$

where α is the thermal diffusivity and $t_{0.5}$ is the time when the temperature at the opposite end to the flash reaches its maximum value. This powerful and simple technique allows for the easy determination of thermal diffusivities. However, this technique is not compatible with ion irradiation for nuclear materials testing. The simple model in equation 2.2 cannot account for varying thermal diffusivity along the material. For ion irradiation where only the surface layers experience radiation damage, the effect can not be isolated. Even if the irradiated layer could be isolated, issues emerge. The finite length of the pulse and finite response speed of temperature sensors mean that it may not be possible to accurately measure the time for the heat front to travel. Furthermore, the theoretical model of the flash method assumes the length over which the light energy is deposited is negligible compared to the sample length, an assumption that may not hold for sub- μm thick samples [19]. Other methods, such as that described in Kanamori et al, are even less suitable [20]. In this method, the phase and amplitude shift between the pulsing of a resistive heating element and the measured temperature response is used to determine the thermal diffusivity. Beyond the mechanical issues of adapting this method to ultra-thin films, the standard setup assumes the length of

the sample is enough that it can be treated as infinite, which would clearly not be the case in this situation [20]. While the standard techniques for thermal diffusivity measurement exclude the use of heavy ion irradiation for determining the evolution of thermal properties for irradiation, transient grating spectroscopy offers a way forward.

Transient grating spectroscopy (TGS) is a powerful tool that allows for rapid iteration and experimentation, through simple and in-situ measurement of thermal diffusivity and tune-able probe depths on the same order as heavy ion damage.

In TGS, the overlapping two pulsed laser beams of wavelength λ at an angle θ on the surface of a sample creates an interference pattern of light and dark regions. The illuminated regions will heat up and expand creating a raised grating, with a spacing, Λ given by

$$\Lambda = \frac{\lambda}{2 \sin\left(\frac{\theta}{2}\right)} \quad (2.3)$$

This rapid expansion further creates two counter-propagating surface acoustic waves (SAWs) of wavelength Λ . A probe laser beam is diffracted off of the grating, allowing for the decay of the SAWs and grating to be measured. Material elastic properties can be extracted from SAW measurement, and the decay of the thermal grating provides information on the thermal diffusivity [21]. Figure 3.5 shows an example of the fit on TGS data.

In order to create the two pump beams necessary to create the thermal grating, a pump laser is passed through a diffraction grating with spacing L , and the first order diffraction beams are used. They pass through an achromatic doublet, resulting in their angle incoming to the sample being the same as leaving from the diffraction grating. This optical configuration results in the relationship between the surface grating spacing Λ and the initial grating spacing,

$$\Lambda = \frac{L}{2} \quad (2.4)$$

Since the probe depth L_{th} of TGS measurement is given by

$$L_{th} = \frac{\Lambda}{\pi} \quad (2.5)$$

the measurement depth can be tuned by manipulating the initial diffraction grating [12]. In this system two probe beams are produced from a single source, which are set 180 degrees out of phase, allowing for their readings to be heterodyned.

To extract thermal properties from TGS data, fits must be made of the phase grating. The phase grating signal is given by

$$I_p(t) = A[\text{erfc}(q\sqrt{\alpha}t) - \frac{\beta}{\sqrt{t}}\exp(-q^2\alpha t)] + B\sin(2\pi ft + \theta)\exp(-\frac{t}{\tau}) + C \quad (2.6)$$

where $I_p(t)$ is the , $q=\frac{2\pi}{\Lambda}$ is the grating wavefunction, A, B and C are amplitude constants, β is a constant describing the ratio of displacement and reflectivity contributions to the grating, f is the acoustic frequency, θ is the acoustic phase, τ is the acoustic decay constant, and α is the thermal diffusivity. A least squares fit can be used to determine these constants from experimental data if the general expected response is known [22].

Figure 2.1 shows an example TGS setup for in-situ measurement during irradiation, showing the phase mask where the initial diffraction grating spacing L can be selected to choose probe depth, the pump and probe lasers, as well as an off-axis ion beam used to irradiate the TGS measurement spot. Due to the non-contact and non-destructive nature of TGS, a setup such as this allows for the changing thermal diffusivity of a sample under ion irradiation to be tracked continuously, providing more granular measurement, and more importantly, ensuring that effects present only during irradiation are captured.

TGS is a proven technique for the applications used in this study, having previously used to measure the thermal diffusivity of helium ion implanted tungsten-rhenium alloys [23]. This study demonstrated many of the benefits of TGS, such as the need for no surface

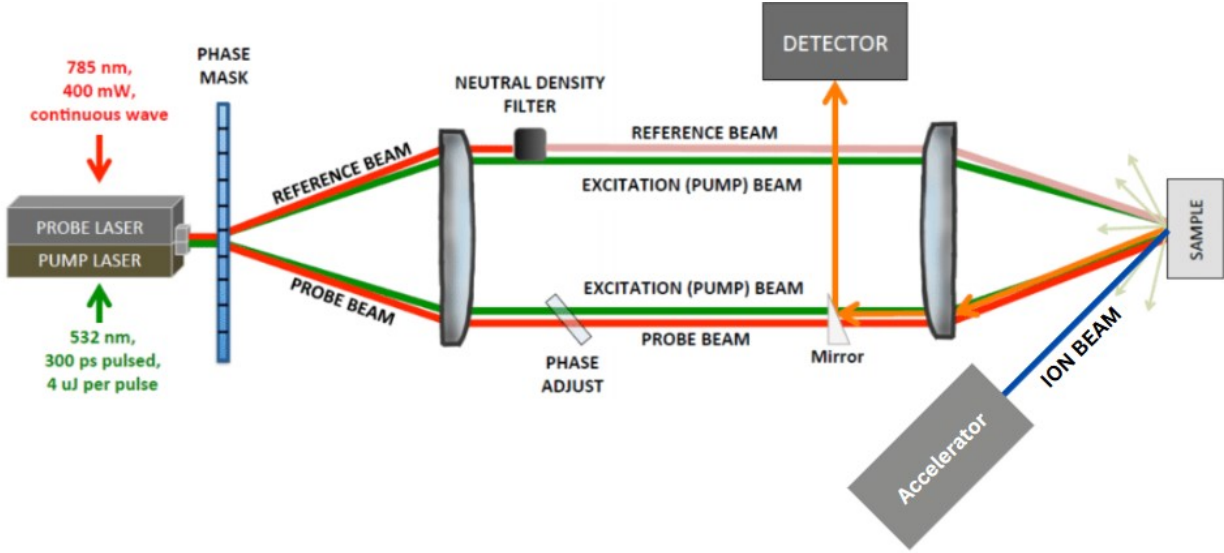


Figure 2.1: Diagram of a TGS setup on an accelerator beamline. Adapted from diagram by Cody Dennett and the MNM Group

preparation beyond polishing, and the ability to select probe depth so as to only capture the ion-implanted range. TGS has also been used in self-ion irradiation studies, with Reza et al using TGS measured thermal diffusivity in self-ion irradiated tungsten to correlate thermal diffusivity with point defect density [24].

Chapter 3

Methods

3.1 Experimental method

In this study, four compositions of tungsten-tantalum alloy were examined: pure tungsten, and tungsten alloys with 3%, 6%, and 11% weight content of tantalum. Each sample is a pure solid solution, with no detectable impurities, and no secondary phases present. For the pure W, 6%, and 11% samples, compositions were confirmed with XRF by AMG Superalloys UK Limited, as shown in table 3.1. All samples are polished mirror-smooth for experimentation, up to a $0.05 \mu\text{m}$ alumina grit. Samples were rectangular pieces, approximately 5x5x1 mm, as shown in figure 3.1.

Measurements were performed on the PI³ (Plasma and Ion Irradiation In-Situ) TGS beamline on the CLASS tandem accelerator at the Massachusetts Institute of Technology. The PI³ beamline consists of a sample holder where the laser beams from an integrated TGS system and the ion beam produced by CLASS can be aligned, allowing for the evolution of

Table 3.1: Measured Sample Compositions by XRF

Element	Pure W	W-6%Ta	W-11%Ta
W	99.99%	94.11%	88.74%
Ta	<0.05%	5.89%	11.26%

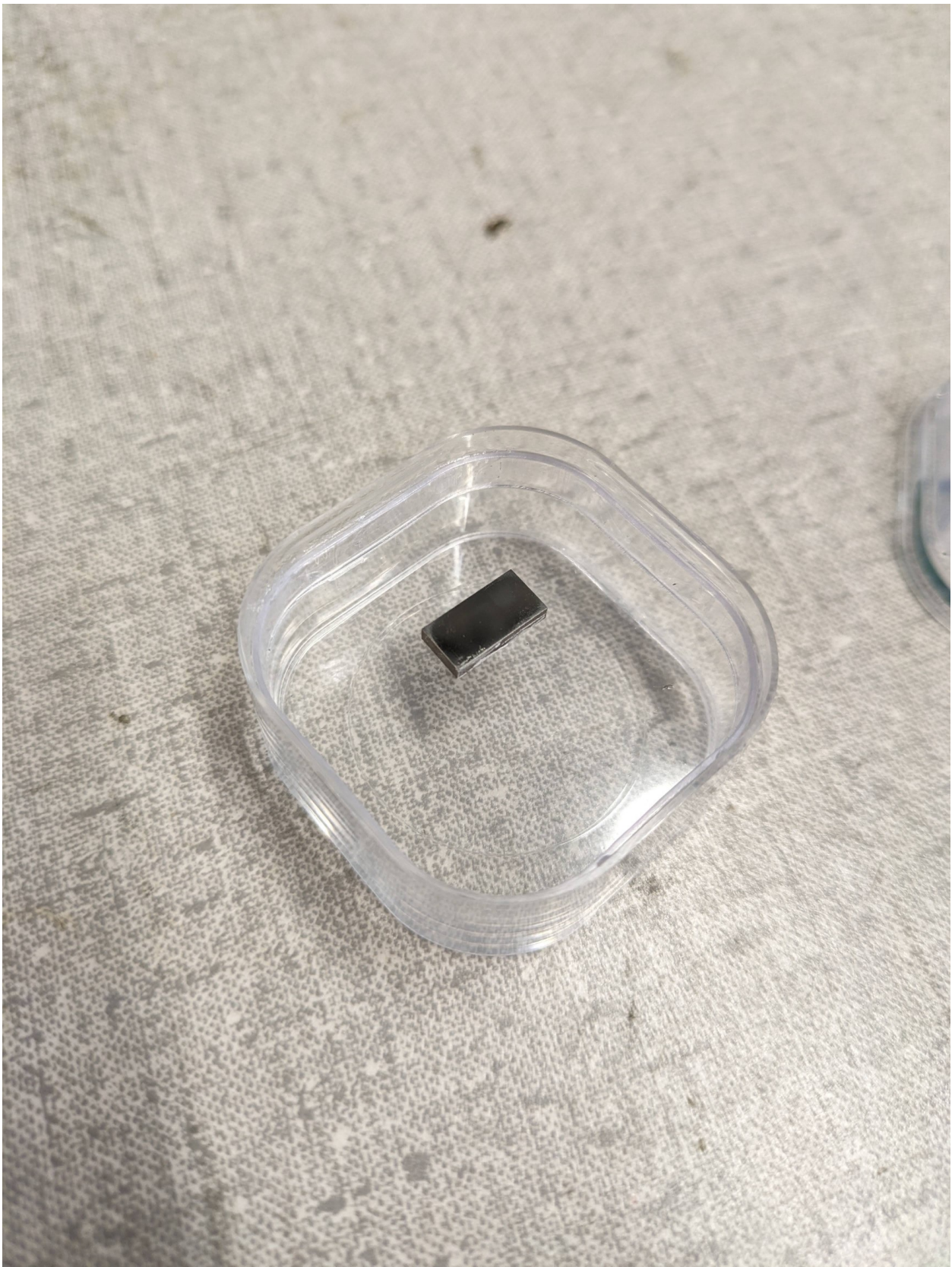


Figure 3.1: W-3%Ta sample

thermal diffusivity during irradiation to be observed, similar to the setup shown in figure 2.1.

On the PI³ TGS system, TGS measurements are taken normal to the sample surface, while the ion beam is at a 45° angle to the sample surface, skewing the circular beam cross section to an ellipsoid irradiation area, as shown in figure 3.2

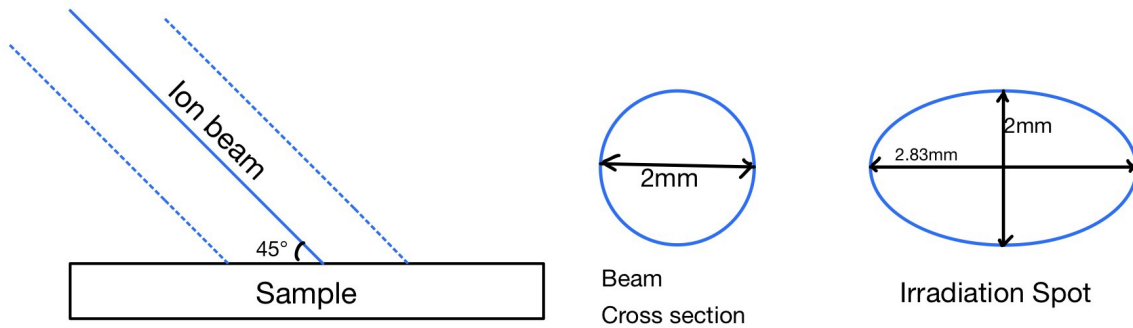


Figure 3.2: Skew of off-axis ion beam

All samples were investigated using the same experimental procedures. First, a calibration run was performed to determine the true grating spacing Λ' on the TGS system, necessary to determine the probe depth L_{th} and ensure proper depth.

Once calibration is complete, the alloy sample is placed in the target chamber, placed on the holder next to a phosphor coated alumina chip used for ion beam alignment, as shown in figure 3.3. The sample was irradiated 10.26 MeV W⁵⁺ beam, which results in approximately a 1 μm damage depth, determined with SRIM as seen in figure 3.4. The beam was narrowed by use of a 2 mm diameter aperture, resulting in a 4.443 mm² irradiation area. Current was measured using an in-line faraday cup. After using the phosphor coated chip to align the ion beam and TGS measurement spot, the beam was blocked, and sample realigned. Continuous TGS measurement was begun, with each thermal diffusivity data point consisting of one minute of averaged measurement. After 10 minutes of measurements, the beam is unblocked, and the sample is irradiated for approximately one hour. The irradiation is completed by lowering the faraday cup and taking a final beam measurement. The specifics of irradiation are shown in table 3.2.

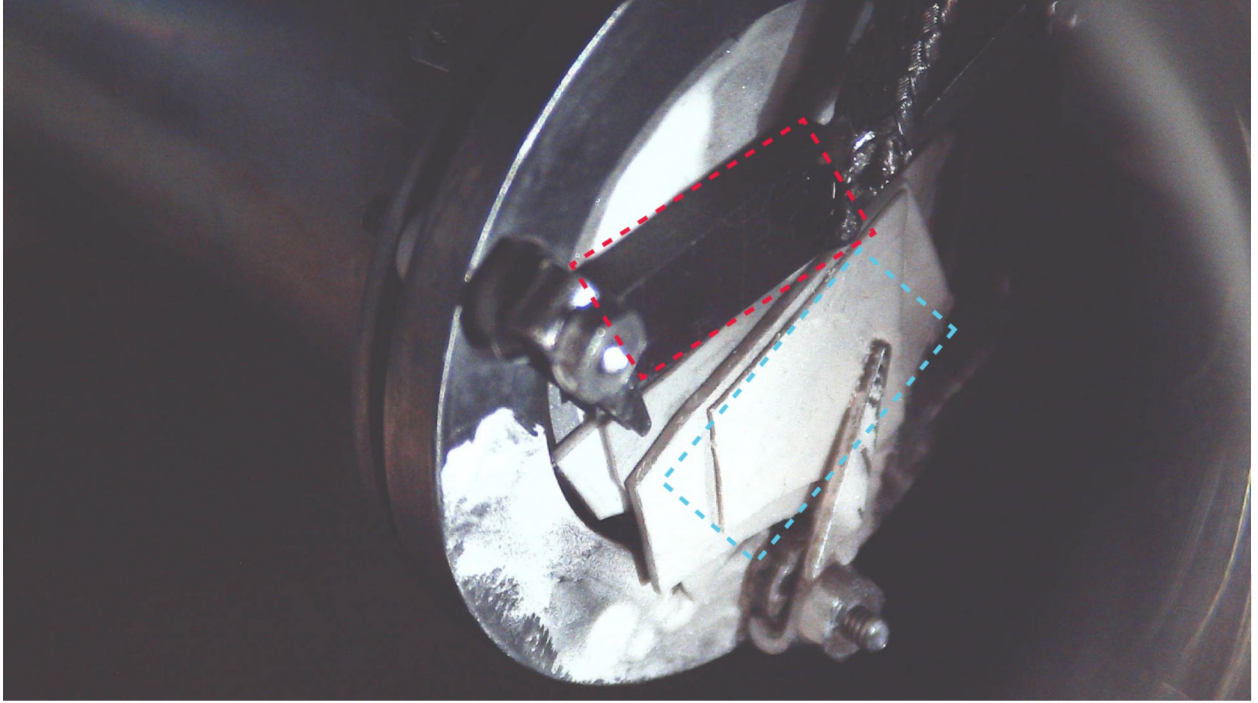


Figure 3.3: Sample holder. Red outline shows sample and blue outline shows phosphor alignment chip

Table 3.2: Sample irradiation parameters

Sample	Start Beam Current (nA)	End Beam Current (nA)	Irradiation Time (min)	Total damage (dpa)
W-6%Ta	6.6	6	77	2.19
W-11%Ta	3.6	3.6	75	1.17

The TGS system is set with a $3.4 \mu\text{m}$ grating spacing. During the TGS measurement phase, measurements are taken continuously at a single spot. Measurements are averaged over one minute to produce a single time-stamp trace, which is later processed.

SRIM-2013 (Stopping Range of Ions in Matter) was used to calculate the damage experienced by the sample over the course of irradiation, allowing for thermal diffusivity to be plotted against displacements per atom. The standard procedure used in Stoller 2013 was used to determine the produced vacancies [25]. The ion beam fluence is calculated based on the spot size and current measured on the faraday cup, and this is used to convert the vacancy calculations to dpa, which is then averaged over the probe depth, and integrated

over total current to find the dpa at each measurement time stamp. Figure 3.4 shows an example the depth profile of sample damage calculated in this method.

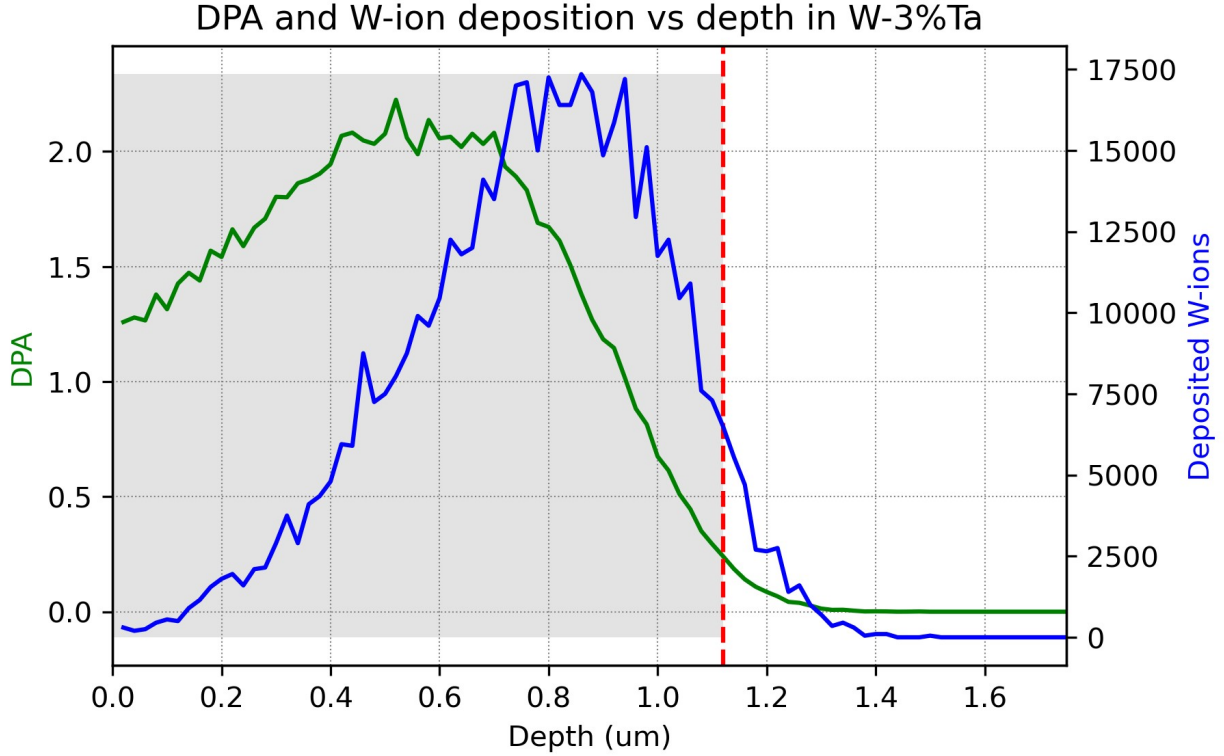


Figure 3.4: dpa and W-ion deposition at various sample depths in 10.26 W^{+5} irradiated W-3%Ta alloy. The shaded region indicates the region measured by the TGS probe

3.2 Analytical Methods

In order to extract useful information from raw TGS data, the signal trace must be fitted to equation 2.6. This is done with a script developed by C.A. Dennett that performs an iterative least-squares fit in order to determine the equation parameters. An example of such a fit can be seen in figure 3.5. The black trace is the raw TGS data, determined from the combination of the two probe signals. The red trace is the functional fit, containing information about the surface acoustic waves and the thermal diffusivity. The blue curve traces out the decay of the grating signal, and thus indicates the thermal diffusivity.

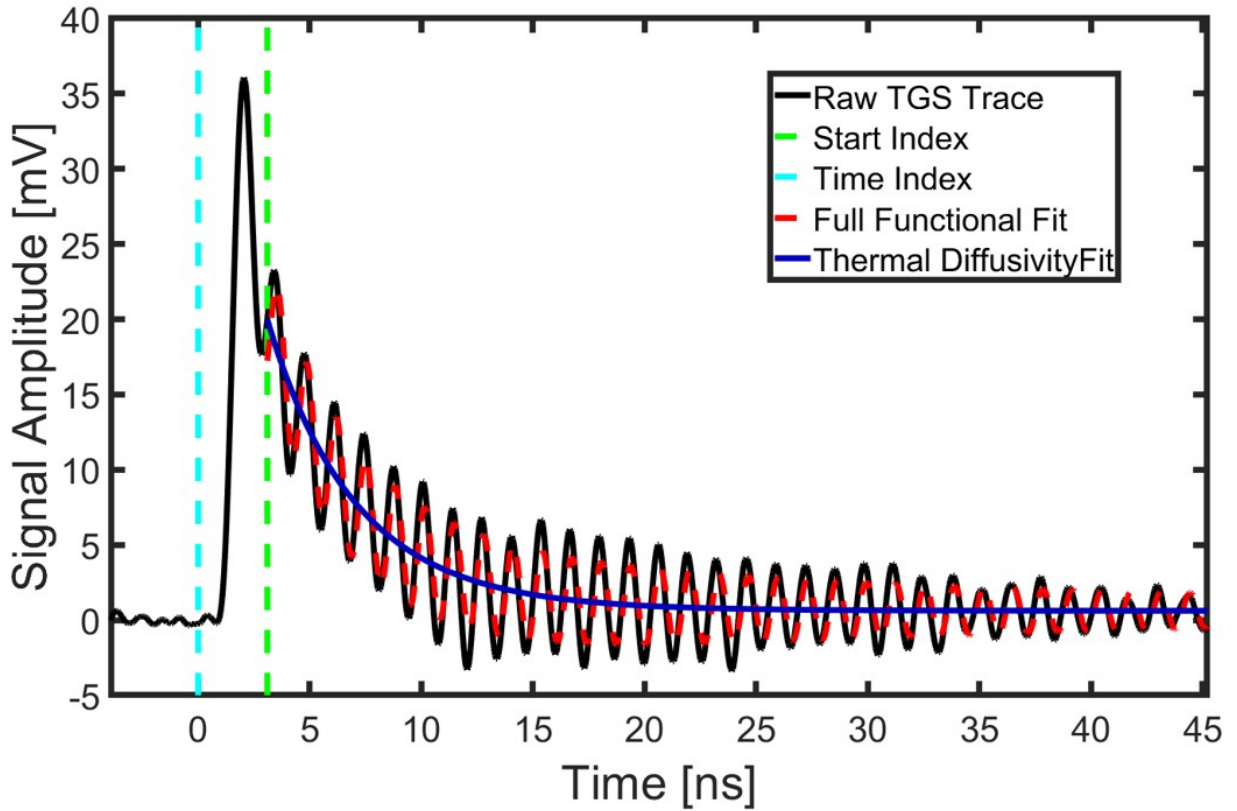


Figure 3.5: TGS signal fit on pure W, showing the thermal decay and surface acoustic wave response

This fit requires that the grating spacing be provided. However, the nature of the initial diffraction grating means that it is not possible to precisely select the grating spacing. Instead, it must be calibrated. To do so, TGS measurements of a single crystal sample of tungsten are performed, and a fit is made with an approximately accurate grating spacing. Since the TGS characteristics of single crystal tungsten are well known and steady, the true grating spacing in meters, Λ' can be determined by

$$\Lambda' = \frac{2669.5}{f} \quad (3.1)$$

where f is the determined surface acoustic wave frequency and 2669.5 is the acoustic wave speed in tungsten in m/s [26]. This true grating spacing is then used as an input to fit TGS measurements taken with the same diffraction grating setting.

Chapter 4

Results

4.1 TGS traces

Figures 4.1 and 4.2 show the TGS traces and fits for representative runs before irradiation and after saturation. There are some variations between samples, such as tightening or greater prominence of the surface acoustic waves. The most notable change is that the thermal fit becomes shallower after irradiation. Since the thermal diffusivity has dropped, the thermal features will fade more slowly, explaining this behavior.

4.2 Observations

Fits to TGS data for each material sample were used to determine the thermal diffusivity at each measurement, which was correlated with the dpa at that timestamp in order to plot the behavior of thermal diffusivity during irradiation for each alloy. The initial unirradiated measurements for each sample were averaged to create the 0 dpa measurement point. The range 0.9-1 dpa exclusive was chosen as a representative "equilibrium" range to allow for comparison before and after irradiation. For the unirradiated and 0.9-1 dpa data points, the error was determined by finding the standard deviation of the averaged values. For the individual points taken during irradiation, the error is the fit error given by the TGS script.

These errors are shown in figure 4.3 as a shaded band. Due to their small magnitude, this band is barely visible.

In all alloy compositions, two primary trends can be seen. The first is a significant drop in thermal diffusivity due to irradiation. The second is the rapid saturation in radiation damage for all samples. By 0.5 dpa of damage, all samples effectively reach their minimum thermal diffusivity values. However, with increasing weight percentage of tantalum comes a corresponding decrease of impact of irradiation on thermal diffusivity. By 1 dpa, pure tungsten has been shown to experience a 46.2% drop in thermal diffusivity. The alloy with 3% tantalum experiences a 36.8% drop, 6% tantalum alloy experiences a 30.1% and 11% wt. tantalum alloy has a 31.0% drop. As a result, thermal diffusivity in pure tungsten goes from being 48.6% higher than in tungsten with 11% tantalum to only being 35.3% greater.

4.3 Experimental Challenges

Many challenges were faced over the course of this study. The primary challenge, and the main source of uncertainty in the results, is the difficulty in aligning the accelerator and TGS beam spots, and in verifying beam current.

To benchmark these results with other studies, the measured thermal diffusivity needs to be correlated to a given dpa value. DPA can be effectively determined with the use of SRIM if the beam current and spot size are known at each TGS measurement timestamp. However, these two variables, along with beam alignment, are a challenge to determine.

Beam non-alignment can result in the overestimation of dpa values. Since the beam is roughly gaussian, the edges of the beam spot will experience lower damage, so an improper alignment would result in insufficient damage. This alignment was a major chokepoint in experimentation, as the limited degrees of freedom of beam alignment and sample adjustment meant that the system often had to be brought out of vacuum for manual adjustment before final alignment could be performed. Determining the beam spot is dependent on the sample

angle and the precision of the aperture. There is less uncertainty but still imprecision.

Another large challenge was determining beam current. The initial procedure was to measure using a current probe on sample, but noise issues prevented this from being used. The procedure implemented is to place a Faraday cup after the aperture before and after irradiation to determine beam current. This places a ceiling on the received current, and when beam spot is small, should effectively determine the beam on sample. However this will count beam that may miss the sample, and lacks granularity over the course of the irradiation.

These factors mean that while the thermal diffusivity values themselves have a high level of confidence, what dpa values they correspond to have undeniable drifts. However, the rapid saturation of thermal diffusivity dropoff indicates valid conclusions can still be drawn.

Figure 4.1: TGS traces for unirradiated samples

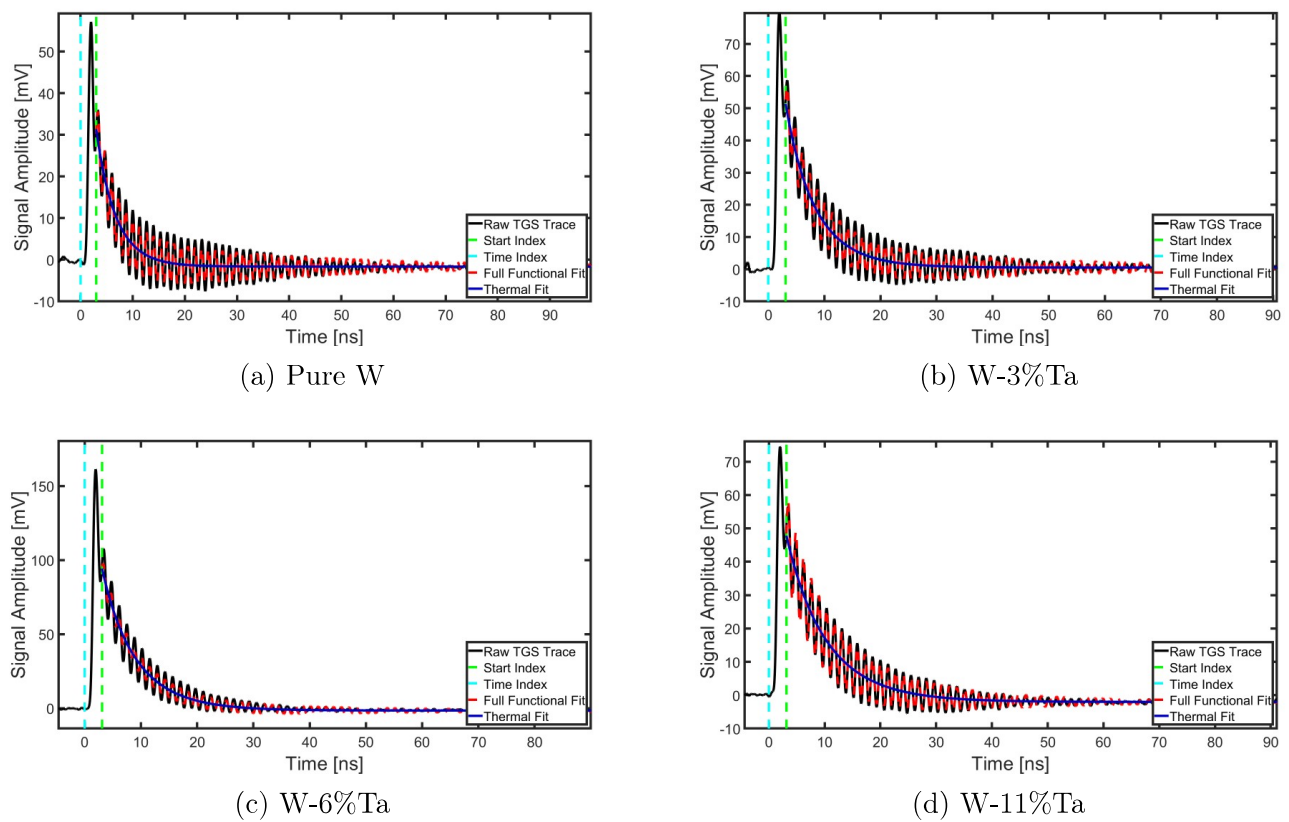
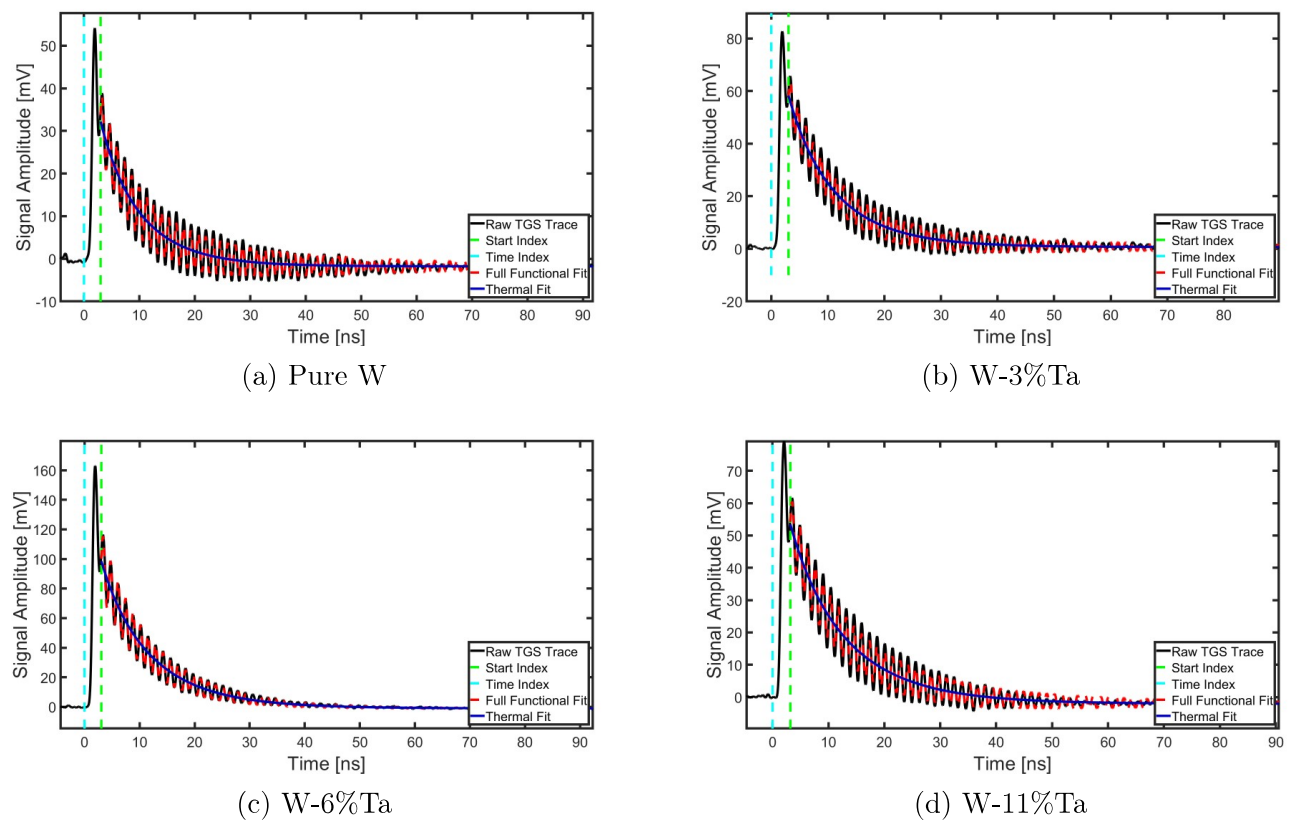


Figure 4.2: TGS traces for samples at saturation



Thermal diffusivity vs dpa in self-ion irradiated W-Ta alloys

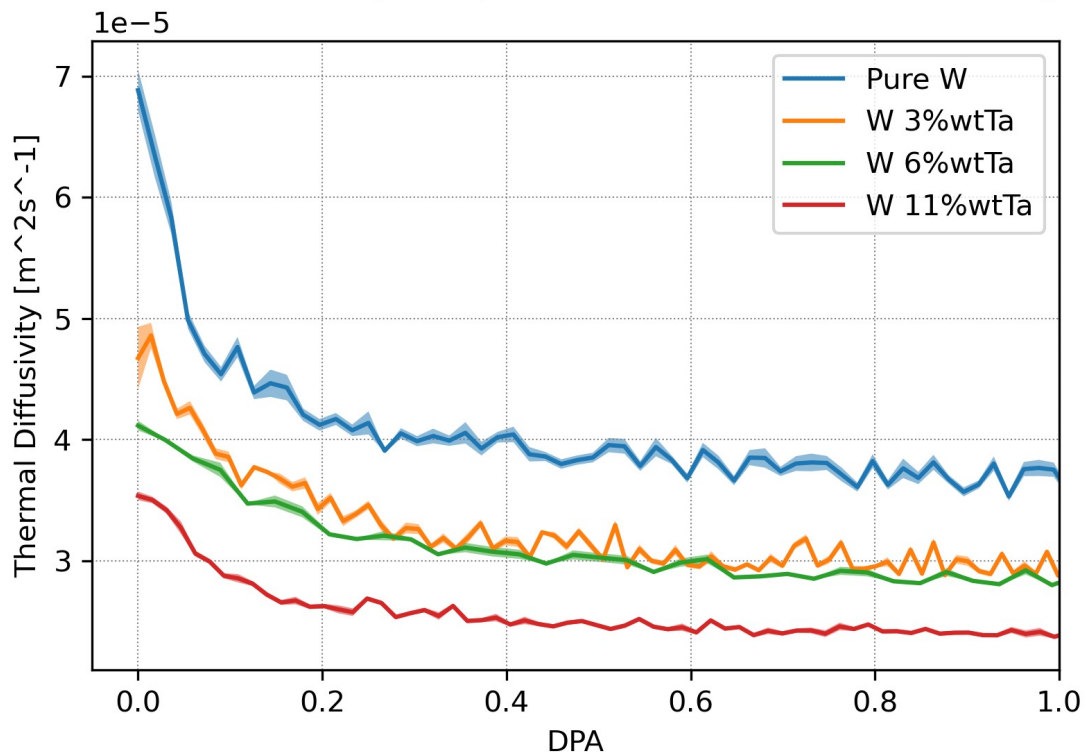


Figure 4.3: Evolution of thermal diffusivity of tungsten-tantalum alloys under self-ion irradiation

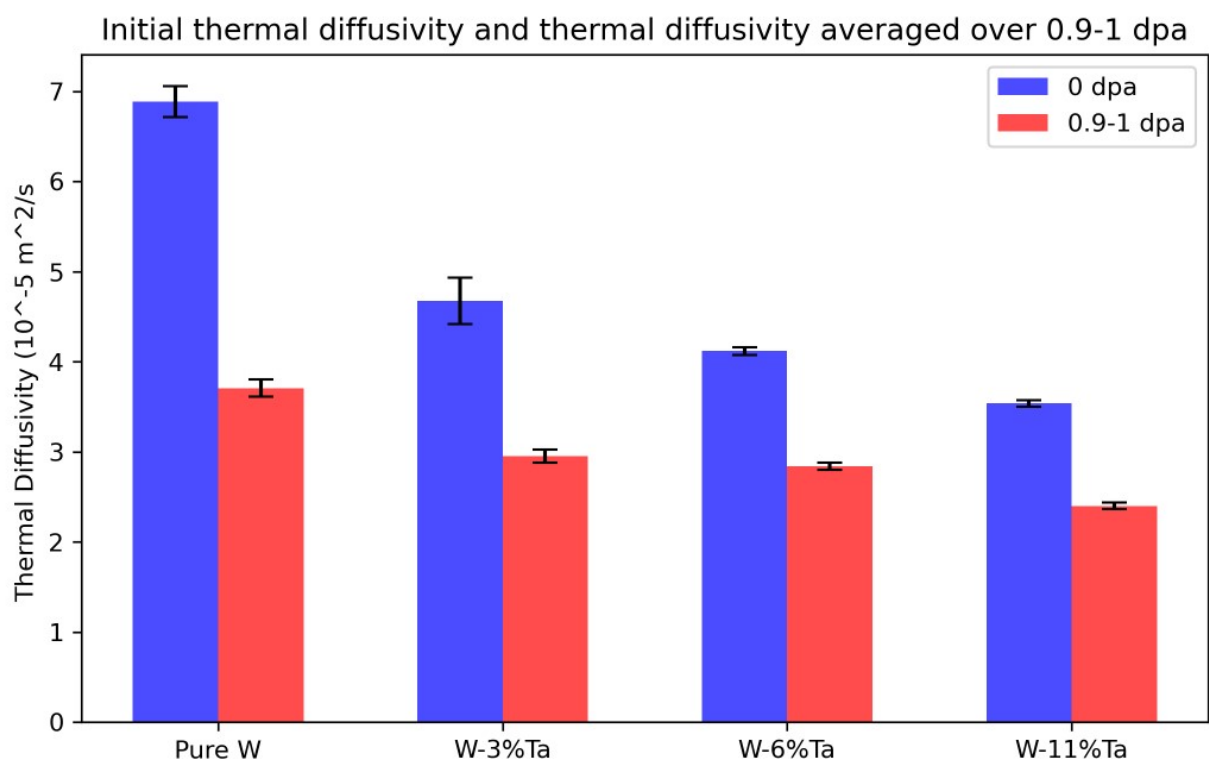


Figure 4.4: Comparison of initial thermal diffusivity with thermal diffusivity after saturation (averaged over 0.9-1 dpa)

Chapter 5

Discussion

While the effects of irradiation on the thermal diffusivity on tungsten-tantalum alloys had not been previously established, the initial thermal diffusivity of the various alloy compositions matches the trends seen in Nogami 2022 [8]. While this study did not analyze 6% or 11% tantalum concentrations, a steady drop in thermal diffusivity from $69 \text{ mm}^2/\text{s}$ to $45 \text{ mm}^2/\text{s}$ is seen going from pure tungsten to tungsten with 5% wt concentration of tantalum, a trend continued here. This initial drop is expected as alloyed materials generally have lower thermal diffusivity than pure materials [8]. Furthermore, various experiments and simulations show that increasing tantalum concentration improves the resilience of to irradiation [7][8][27]. The Yang study shows that the attractive interaction of Ta-Re pairs and repulsion between Ta and Re self-interstitials in W act to reduce Re mobility and cluster stability, reducing Re clustering [7]. Nogami experimentally showed a reduction in irradiation hardening [8]. Ipatova showed that tantalum addition reduced void mobility and thus delayed void formation and accompanying swelling [27]. While the primary improvements are in mechanical properties, behaviors such as the reduction of lattice disruptions may enhance thermal diffusivity by increasing phonon transport [28].

The TGS measurements of thermal diffusivity in tungsten irradiated by 20 MeV W ions in the study by Reza et al can be used as a benchmark for these results. Figure 5.1

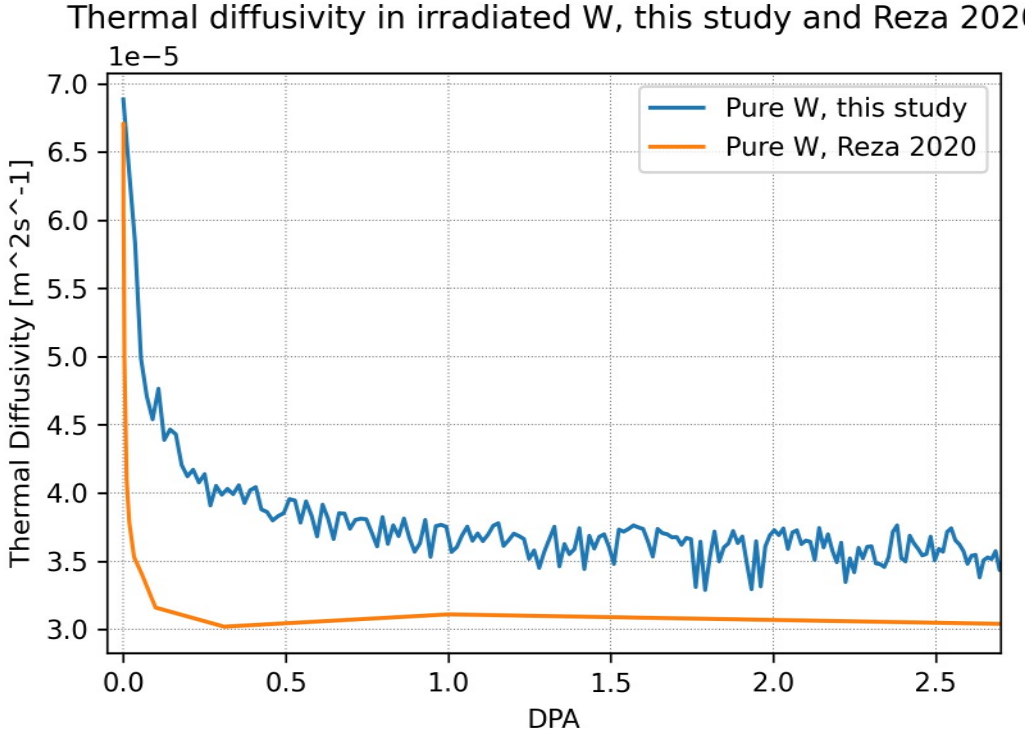


Figure 5.1: Comparing the evolution of W thermal diffusivity across studies

shows the two traces overlaid. Compared to what is seen here, a much sharper fall off in thermal diffusivity can be seen in the data from Reza 2020 compared to the measurements in this study. Given the similar curves seen in this study’s data, it is likely that this discrepancy is a result of overestimating the irradiation damage on the measured sample area, not of a true difference in behavior. However, this would not affect the measured thermal diffusivity values or their measured changes [24].

This initial drop in thermal diffusivity is due to the disruptions produced by irradiation, particularly the formation of point and loop defects [24]. In tungsten, some of the heat transfer is due to phonons travelling through the crystal lattice. Irradiation induced defects that disrupt the lattice and thus the transfer of phonons, and thus reduce the thermal diffusivity [28]. Tantalum has been shown to suppress the formation of these lattice defects, and thus tantalum addition could be assumed to reduce the magnitude of the thermal diffusivity drop due to irradiation. Tantalum also suppresses transmutation product clustering. Since no

transmutation products are produced or introduced through self-ion irradiation, this study does miss the thermal effects of reduced clustering.

One notable observed result was the saturation of thermal diffusivity drop at 0.5 dpa. Given that the DEMO divertor is estimated to be damaged at a rate of 3 dpa per full power year, the divertor will achieve equilibrium thermal diffusivity in less than two months of full power operation [3]. As a result, it is only reasonable for design considerations for divertor material selections to consider the irradiated state, where the negative impact on thermal properties with increasing tantalum fraction is reduced.

This saturation in thermal damage matches well with the saturation in nanohardness and loop defect density achieved at around 0.5 dpa seen in studies of self-irradiated tungsten [29]. Since lattice disruptions result in the thermal diffusivity drop, a saturation in these disruptions would result in the observed saturation of thermal diffusivity degradation. Further microscopy analysis of irradiated samples to determine defect evolution, as well as a better understanding of the mechanics of saturation is needed to fully understand this evolution.

Various clear next steps can be taken to further this investigation. The first is to measure the thermal diffusivity properties of irradiated alloys at higher temperatures. ITER's divertor is expected to reach peak temperatures of approximately 1100 C [30]. Reaching higher temperatures could better illustrate more relevant behavior. Furthermore, existing research shows that the gap between thermal diffusivities of different tungsten-tantalum alloy compositions narrows with increasing temperature [8]. Observing the combination of this narrowing with that resulting from irradiation would provide new insights. Another clear pathway to move forward is the use of finite element modeling to determine the behavior of these alloys in fusion reactor conditions. This modeling could identify how the improvement in mechanical properties granted by tantalum addition is balanced out by the decrease in thermal properties in practice.

Chapter 6

Conclusion

Figure 4.4 perfectly demonstrates the key takeaway of this study. Before irradiation, a dramatic fall-off in thermal diffusivity with increasing tantalum concentration can be observed. This drop might have led fusion power plant designers to discount tungsten-tantalum alloys as plasma facing materials. The mechanical property and irradiation resilience advantages granted by adding tantalum might not counterbalance the significant thermal penalty. However, at damage levels reached in a fraction of the planned lifetime of these materials, the gap in measured thermal diffusivity shrinks dramatically.

This study serves as an important stepping stone moving forward. Not only does this demonstrate the increased viability of tungsten-tantalum alloys in fusion applications, it also provides invaluable data for the prediction of the behavior of these materials over their lifetime in a fusion power plant. Furthermore, the combination of TGS and heavy ion irradiation as a method for analyzing the evolution of thermal diffusivity under irradiation has been validated.

From here, the path for optimizing the use of tungsten-tantalum alloys in fusion reactors can be seen, and major steps can be taken in overcoming the material challenges that must be overcome for economical fusion power to be a reality.

Appendix A

Transmutation and realistic irradiation of Tungsten-Tantalum alloys

A.1 Motivation

This study investigated the effects of irradiation on tungsten-tantalum alloys, tracing the evolution of thermal diffusivity as radiation damage builds up. However, this study does not take into account a vital phenomenon for fusion reactor materials - the creation of transmutation products.

This effect is significant in plasma facing materials. In a 14.1 MeV neutron flux, tungsten is transmuted into elements such as rhenium, osmium, and tantalum. By the end of its life, an initially pure tungsten component could have as high as 3.8% Re, 1.38% Os, and 0.81% Ta [6]. The production of rhenium is a particular issue, with rhenium clustering leading to embrittlement [7]. While the prevention of transmutation product clustering is a major motivator for tantalum addition, transmutation means that considering only pure tungsten-tantalum alloys under irradiation will not paint the full picture, and will miss the effects of these new species on material properties.

Since the transmutation and radiation damage effects produced in a fusion reactor cannot

be produced otherwise, heavy ion irradiation cannot be used directly to emulate the combined neutron irradiation effects. However, by identifying the transmutation-altered composition corresponding to a given damage level, this issue can be overcome. A sample can be prepared with that end-state composition, then be self-ion irradiated to the target damage level, and properties measured. This method has been used before, such as in the study of helium-implanted tungsten-rhenium alloys. By creating samples with the level of rhenium that would be created through transmutation, the effects of helium gas generation could be simulated without a fusion neutron source [23].

A second factor that needs to be taken into account is the spatial variation of damage and transmutation. Absorption, moderation, and scattering mean that each point along a fusion material will experience a different neutron flux, and thus different levels of damage, and the properties of components will vary not only in time but in space.

This section uses simulations to study both of these effects on the tungsten-tantalum alloys examined in this study, to help paint a more complete picture of the behavior of these alloys in a fusion environment, and to help select pathways for future experiments that will extend the combination of self-ion irradiation and TGS to cover the entire evolution of these alloys in a fusion environment.

A.2 Methods

Two simulation tracks are taken, the first being the use of GEANT-4 through the Grasshopper front end, and the second being the use of FISPACT-II.

GEANT-4 is a monte carlo particle simulation code developed by CERN, which analyzes the interaction of particles with matter. It is a rich code, including ion, neutron, and photon interactions. GEANT-4 is used here to track the spatial behavior of fusion neutron interactions with tungsten-tantalum alloys, tracking scattering and transmutation to determine spatial variation in energy deposition and transmutation events. Grasshopper is a front

end to GEANT-4, developed at MIT to simplify its use. This front end takes in an XML file description of the simulation parameters, and produces an easily parseable ROOT file. Grasshopper is used to define the simulations cases here [31].

FISPACT-II is an inventory code that tracks transmutation. It takes in information about sample composition and neutron flux, and with cross section tables and decay information, it solves the radioactive decay equations to determine the evolution of material composition. It is used here to determine the bulk transmutation of tungsten-tantalum alloys under fusion irradiation over their lifetime.

A.2.1 Grasshopper

The ITER divertor is made of tungsten monoblocks, 28x28x12 mm components with a central coolant channel [32]. Since the goal of this study is to determine the dependence of transmutation product generation on depth from the first surface, the interaction object will be a 28mm cube. The flux on the surface is assumed to be roughly even, so a pencil beam of 14.1 MeV neutrons with a 20mm diameter will be used. 1000000 particles are used, and Geant4 is set to SaveTrackInfo mode in order to determine the position of transmutation events. Four material compositions are used: a pure tungsten, and tungsten with 3%, 6%, and 11% tantalum composition, and the simulation run for each, producing a ROOT output file. Figure A.1 shows the simulation geometry.

To determine the distribution of events, the z-position of neutron capture and inelastic neutron reactions are histogrammed, with naturally existing tungsten and tantalum isotopes, as well as neutrons and gammas are removed. This leaves only the transmutation products that would affect the material's properties.

In a root environment, the following commands are used to produce the graph

```
1 tree->Draw("z_incident -36>>eventHist(100,-1,30)", "(ParticleName!="
neutron"&&ParticleName!="gamma")&&(CreatorProcessName==""
neutronInelastic"||CreatorProcessName=="nCapture")&&(
```

```

1 ParticleName != "Ta181" && ParticleName != "W180" && ParticleName != "
2 W182" && ParticleName != "W183" && ParticleName != "W184" ) )

3 eventHist -> SetTitle( "Transmutation events in pure W under 14.1 MeV
4 neutron irradiation" )

5 eventHist -> GetXaxis() -> SetTitle( "Depth(mm)" )

6

7 eventHist -> GetYaxis() -> SetTitle( "Counts" )

```

A fourth degree polynomial is then fit to the histogram to better trace out the behavior.

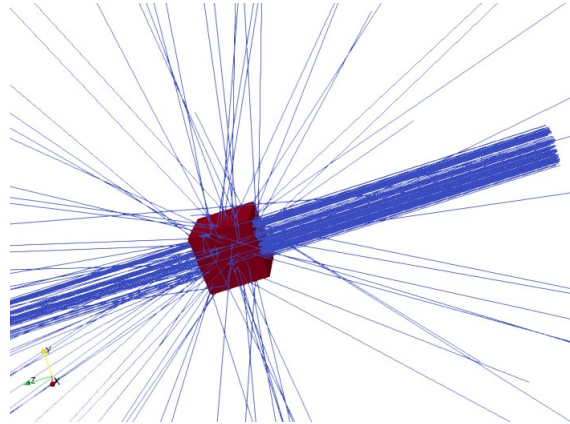


Figure A.1: Geant4 simulation of 14.1 MeV neutrons interacting with a 28 mm thick tungsten alloy block

A.2.2 FISPACT-II

Four simulations are run, each corresponding to one of the alloy compositions. The fusion neutron spectrum provided in the FNSInconel example file is used, and a wall loading of $1.04 \times 10^{14} n/cm^2$, corresponding to that determined by the Power Plant Conceptual study, is used [9]. The simulations are run to capture behavior over 1000 days of irradiation. The simulations are run at timesteps of 1, 10, 100, and 1000 days. The top 5 final elements (W, Ta, Re, Os, Hf) are plotted over each time step.

Table A.1: Pure W element weight fraction evolution over irradiation

Element	Start	1 day	11 days	111 days	1111 days
W	1	1	1.00E+00	9.97E-01	9.24E-01
Ta	0	5.57E-07	1.91E-05	1.30E-03	3.77E-02
Re	0	6.21E-07	3.70E-05	1.86E-03	3.58E-02
Os	0	1.21E-12	4.79E-09	1.90E-06	3.20E-04
Hf	0	5.66E-08	6.19E-07	1.03E-05	1.68E-03

A.3 Results

A.3.1 Grasshopper

Figure A.2 shows the distributions of transmutation events with depths for varying tungsten-tantalum alloys as determined in the GEANT-4 simulations. In all of the alloy composition, a clear spatial distribution can be seen. The density of transmutation events rises to peak at around an 8mm depth, then falls off gradually to the end of the material. There are slight variations in this trend between the materials, with W-11%Ta having the most prominent peak, though only barely. However, the variation remains prominent, and would result in a notably varying composition across the thickness of first wall materials.

A.3.2 FISPACT-II

Figure A.3 shows the evolution of element concentration over time in various tungsten-tantalum alloys. Tables A.1-A.4, also show this evolution. One can see that the composition varies dramatically, with Ta concentration nearly doubling in some alloys. However, it can also be noted that for the time periods that are represented by the initial thermal diffusivity drop measured in this study, the compositions are mostly unchanged from the initial values.

Table A.2: W-3%Ta element weight fraction evolution

Element	Start	1 day	11 days	111 days	1111 days
W	97E-01	9.70E-01	9.70E-01	9.67E-01	8.96E-01
Ta	3E-02	3.00E-02	3.00E-02	3.09E-02	6.32E-02
Re	0	6.02E-07	3.59E-05	1.80E-03	3.47E-02
Os	0	1.17E-12	4.65E-09	1.84E-06	3.11E-04
Hf	0	1.34E-06	2.40E-05	2.58E-04	4.30E-03

Table A.3: W-6%Ta element weight fraction evolution

Element	Start	1 day	11 days	111 days	1111 days
W	9.4E-01	9.40E-01	9.40E-01	9.37E-01	8.69E-01
Ta	6E-02	6.00E-02	6.00E-02	6.06E-02	8.86E-02
Re	0	5.83E-07	3.48E-05	1.75E-03	3.36E-02
Os	0	1.14E-12	4.51E-09	1.78E-06	3.01E-04
Hf	0	2.63E-06	4.74E-05	5.05E-04	6.92E-03

Table A.4: W-11%Ta element weight fraction evolution

Element	Start	1 day	11 days	111 days	1111 days
W	8.9E-01	8.90E-01	8.90E-01	8.87E-01	8.24E-01
Ta	1.1E-01	1.10E-01	1.10E-01	1.10E-01	1.31E-01
Re	0	5.52E-07	3.29E-05	1.65E-03	3.18E-02
Os	0	1.08E-12	4.27E-09	1.69E-06	2.85E-04
Hf	0	4.77E-06	8.63E-05	9.17E-04	1.13E-02

A.4 Conclusions

This study used self-ion irradiation and TGS to demonstrate that under irradiation, the thermal diffusivity penalty of tantalum addition shrinks dramatically, indicating the greater viability of tungsten-tantalum alloys for fusion reactor applications. However, these alloy compositions do not accurately represent what will be present in a fusion reactor environment. Any tungsten-tantalum alloy will quickly become a tungsten-tantalum-rhenium-osmium alloy with helium filled voids. This composition will vary both with space and time, greatly increasing the complexity of the behavior of these alloys in a fusion environment.

GEANT-4 and FISPACT-II simulations help illustrate these effects. The GEANT-4 simulations clearly show how the density of transmutation event varies across the thickness of the material. This means that the composition and thus properties at the surface interacting with the plasma may be notably different from those at the surface interacting with the fibre blanket.

The FISPACT simulations, run over a 1111 day irradiation -nearly three years- represents the rough lifetime of a divertor component. Dramatic changes in composition are seen at end of life, but at the time scales at which the initial equilibrium in thermal diffusivity is observed, the composition remains mostly unchanged. This shows that the experiments in this study do not provide a view into the entire evolution of first wall materials, but can be considered valid for a not-insignificant fraction of the component's life, when the greatest property change is likely to be observed.

The information gleaned here presents a clear path forward. With this, combinations of DPA, composition, and location can be determined which need to be evaluated. Samples with the corresponding elemental composition can be created, brought to the right dpa through ion irradiation, then TGS used to determine thermal diffusivity. That way, a true picture of the entire behavior of these alloys in a fusion environment can be determined.

Figure A.2: Transmutation events at differing depths for tungsten-tantalum alloys

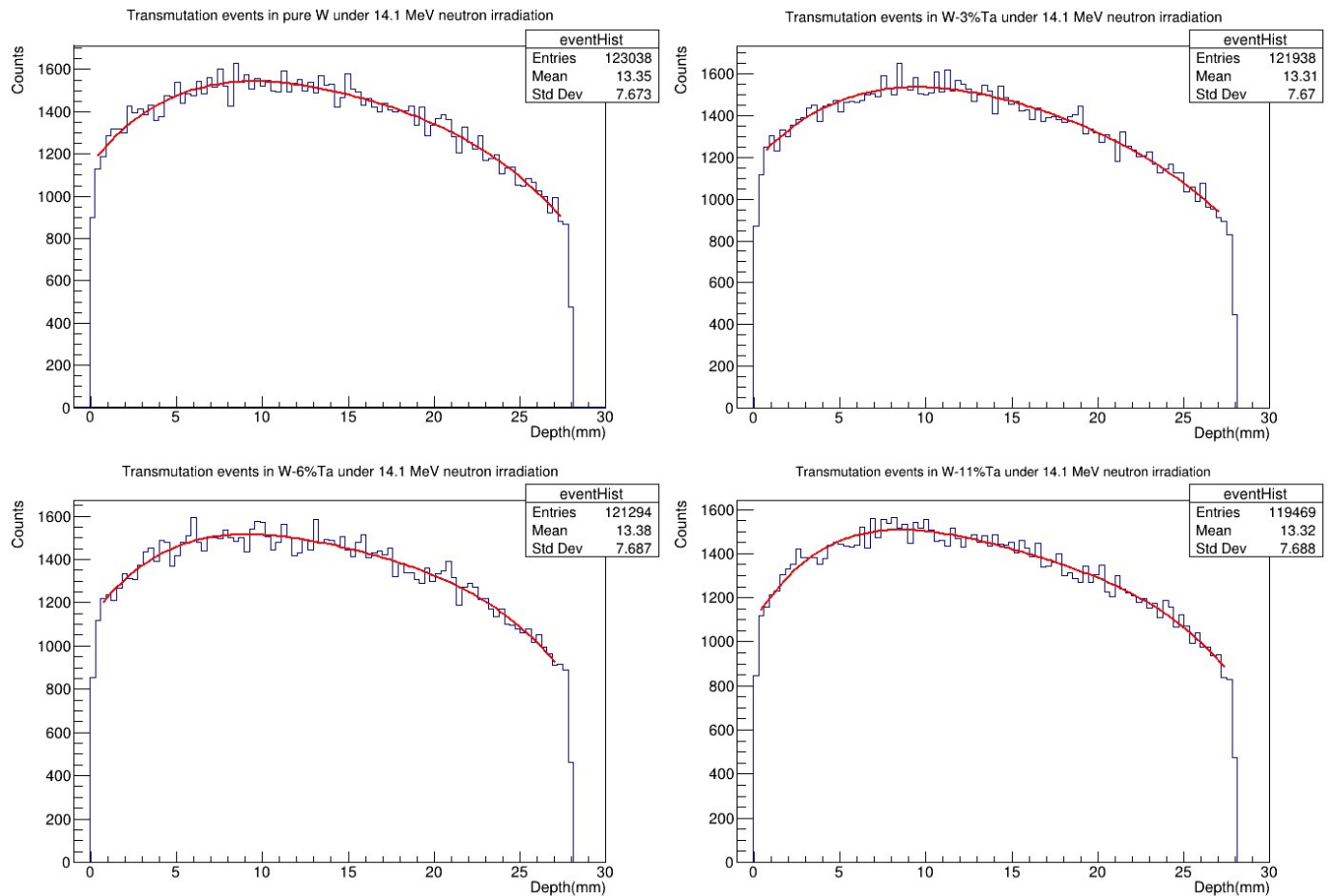
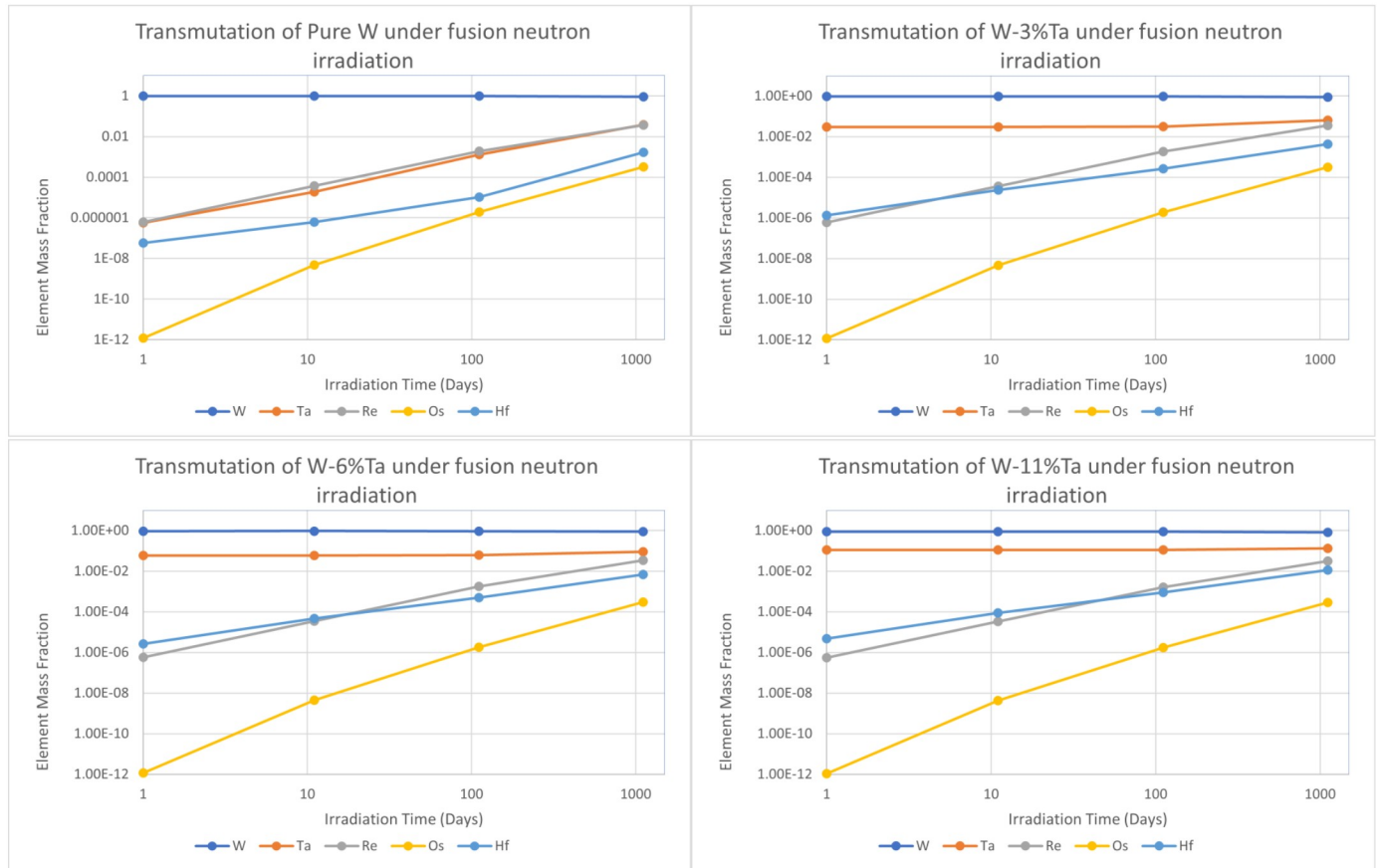


Figure A.3: Composition over time for W-Ta alloys under fusion neutron irradiation



Appendix B

Data Availability

TGS scripting code was taken from: <https://github.com/shortlab/TGS-Processing-Scripts>
Grasshopper code is found at: <https://github.com/ustajan/grasshopper> Figures and files for
this study are found at: <https://github.com/shortlab/2024-eahuactz-thesis>

References

- [1] A. J. Creely, M. J. Greenwald, S. B. Ballinger, *et al.*, “Overview of the SPARC tokamak,” *Journal of Plasma Physics*, vol. 86, no. 5, p. 865 860 502, Oct. 2020, ISSN: 0022-3778. DOI: [10.1017/S0022377820001257](https://doi.org/10.1017/S0022377820001257).
- [2] A. Kuang, N. Cao, A. Creely, *et al.*, “Conceptual design study for heat exhaust management in the ARC fusion pilot plant,” *Fusion Engineering and Design*, vol. 137, pp. 221–242, Dec. 2018, ISSN: 09203796. DOI: [10.1016/j.fusengdes.2018.09.007](https://doi.org/10.1016/j.fusengdes.2018.09.007).
- [3] G. Federici, W. Biel, M. Gilbert, R. Kemp, N. Taylor, and R. Wenninger, “European DEMO design strategy and consequences for materials,” *Nuclear Fusion*, vol. 57, no. 9, p. 092 002, Sep. 2017, ISSN: 0029-5515. DOI: [10.1088/1741-4326/57/9/092002](https://doi.org/10.1088/1741-4326/57/9/092002).
- [4] I. Ipatova, R. W. Harrison, P. T. Wady, S. M. Shubeita, D. Terentyev, S. E. Donnelly, and E. Jimenez-Melero, “Structural defect accumulation in tungsten and tungsten-5wt.% tantalum under incremental proton damage,” *Journal of Nuclear Materials*, vol. 501, 2018, ISSN: 00223115. DOI: [10.1016/j.jnucmat.2017.11.030](https://doi.org/10.1016/j.jnucmat.2017.11.030).
- [5] D. Terentyev, C. Yin, A. Dubinko, C. C. Chang, and J. H. You, “Neutron irradiation hardening across ITER diverter tungsten armor,” *International Journal of Refractory Metals and Hard Materials*, vol. 95, p. 105 437, Feb. 2021, ISSN: 0263-4368. DOI: [10.1016/J.IJRMHM.2020.105437](https://doi.org/10.1016/J.IJRMHM.2020.105437).
- [6] Y. Li, F. Ma, F. Yue, Q. Ren, H. Zhou, and G. Lu, “Radiation-induced precipitation of transmutation elements rhenium/osmium and their effects on hydrogen behavior in

tungsten,” *Progress in Natural Science: Materials International*, vol. 29, no. 3, pp. 285–294, Jun. 2019, ISSN: 1002-0071. DOI: [10.1016/J.PNSC.2019.03.014](https://doi.org/10.1016/J.PNSC.2019.03.014).

- [7] T. R. Yang, Y. H. Li, Y. Z. Niu, F. Y. Yue, G. H. Lu, and H. B. Zhou, “Suppressing effect of tantalum on the radiation-induced clustering of rhenium in tungsten,” *Journal of Nuclear Materials*, vol. 562, p. 153588, Apr. 2022, ISSN: 0022-3115. DOI: [10.1016/J.JNUCMAT.2022.153588](https://doi.org/10.1016/J.JNUCMAT.2022.153588).
- [8] S. Nogami, I. Ozawa, D. Asami, *et al.*, “Tungsten–tantalum alloys for fusion reactor applications,” *Journal of Nuclear Materials*, vol. 566, 2022, ISSN: 00223115. DOI: [10.1016/j.jnucmat.2022.153740](https://doi.org/10.1016/j.jnucmat.2022.153740).
- [9] M. Gilbert and J.-C. Sublet, “Neutron-induced transmutation effects in W and W-alloys in a fusion environment,” *Nuclear Fusion*, vol. 51, no. 4, p. 043005, Apr. 2011, ISSN: 0029-5515. DOI: [10.1088/0029-5515/51/4/043005](https://doi.org/10.1088/0029-5515/51/4/043005).
- [10] S. J. Jepeal, L. Snead, and Z. S. Hartwig, “Intermediate energy proton irradiation: Rapid, high-fidelity materials testing for fusion and fission energy systems,” *Materials and Design*, vol. 200, 2021, ISSN: 18734197. DOI: [10.1016/j.matdes.2020.109445](https://doi.org/10.1016/j.matdes.2020.109445).
- [11] O. V. Ogorodnikova, B. Tyburska, V. K. Alimov, and K. Ertl, “The influence of radiation damage on the plasma-induced deuterium retention in self-implanted tungsten,” *Journal of Nuclear Materials*, vol. 415, no. 1, S661–S666, Aug. 2011, ISSN: 0022-3115. DOI: [10.1016/J.JNUCMAT.2010.12.012](https://doi.org/10.1016/J.JNUCMAT.2010.12.012).
- [12] C. A. Dennett, D. L. Buller, K. Hattar, and M. P. Short, “Real-time thermomechanical property monitoring during ion beam irradiation using in situ transient grating spectroscopy,” *Nuclear Instruments and Methods in Physics Research Section B: Beam Interactions with Materials and Atoms*, vol. 440, pp. 126–138, Feb. 2019, ISSN: 0168-583X. DOI: [10.1016/J.NIMB.2018.10.025](https://doi.org/10.1016/J.NIMB.2018.10.025).
- [13] M. Y. Xu, L. M. Luo, Y. F. Zhou, X. Zan, Y. Xu, Q. Xu, K. Tokunaga, X. Y. Zhu, and Y. C. Wu, “Helium irradiation behavior of tungsten-niobium alloys under different ion

energies,” *Fusion Engineering and Design*, vol. 132, pp. 7–12, Jul. 2018, ISSN: 0920-3796. DOI: [10.1016/J.FUSENGDES.2018.05.015](https://doi.org/10.1016/J.FUSENGDES.2018.05.015).

- [14] J. C. Haley, S. de Moraes Shubeita, P. Wady, A. J. London, G. R. Odette, S. Lozano-Perez, and S. G. Roberts, “Microstructural examination of neutron, proton and self-ion irradiation damage in a model Fe9Cr alloy,” *Journal of Nuclear Materials*, vol. 533, p. 152 130, May 2020, ISSN: 0022-3115. DOI: [10.1016/J.JNUCMAT.2020.152130](https://doi.org/10.1016/J.JNUCMAT.2020.152130).
- [15] A. V. Spitsyn, N. P. Bobyr, T. V. Kulevoy, P. A. Fedin, A. I. Semennikov, and V. S. Stolbunov, “Use of MeV energy ion accelerators to simulate the neutron damage in fusion reactor materials,” *Fusion Engineering and Design*, vol. 146, pp. 1313–1316, Sep. 2019, ISSN: 0920-3796. DOI: [10.1016/J.FUSENGDES.2019.02.065](https://doi.org/10.1016/J.FUSENGDES.2019.02.065).
- [16] D. E. J. Armstrong, A. J. Wilkinson, and S. G. Roberts, “Mechanical properties of ion-implanted tungsten–5wt% tantalum,” *Physica Scripta*, vol. T145, p. 014 076, Dec. 2011, ISSN: 0031-8949. DOI: [10.1088/0031-8949/2011/T145/014076](https://doi.org/10.1088/0031-8949/2011/T145/014076). URL: <https://iopscience.iop.org/article/10.1088/0031-8949/2011/T145/014076>.
- [17] J. H. Yu, H. Kurotaki, M. Ando, and T. Nozawa, “Mechanical properties of self-ion irradiated pure tungsten using nano-indentation test and micro-tensile test,” *Nuclear Materials and Energy*, vol. 30, p. 101 145, 2022. DOI: [10.1016/j.nme.2022.101145](https://doi.org/10.1016/j.nme.2022.101145). URL: <https://doi.org/10.1016/j.nme.2022.101145>.
- [18] H. Bolt, V. Barabash, G. Federici, J. Linke, A. Loarte, J. Roth, and K. Sato, “Plasma facing and high heat flux materials – needs for ITER and beyond,” *Journal of Nuclear Materials*, vol. 307-311, no. 1 SUPPL. Pp. 43–52, Dec. 2002, ISSN: 0022-3115. DOI: [10.1016/S0022-3115\(02\)01175-3](https://doi.org/10.1016/S0022-3115(02)01175-3).
- [19] L. Vozár and W. Hohenauer, “Flash method of measuring the thermal diffusivity. A review,” *High Temperatures-High Pressures*, vol. 35/36, no. 3, pp. 253–264, 2003, ISSN: 0018-1544. DOI: [10.1068/htjr119](https://doi.org/10.1068/htjr119).

- [20] H. Kanamori, H. Mizutani, and N. Fujii, “Method of thermal diffusivity measurement,” *Journal of Physics of the Earth*, vol. 17, no. 1, pp. 43–53, 1969.
- [21] F. Hofmann, M. P. Short, and C. A. Dennett, “Transient grating spectroscopy: An ultrarapid, nondestructive materials evaluation technique,” *MRS Bulletin*, vol. 44, no. 5, pp. 392–402, May 2019, ISSN: 0883-7694. DOI: [10.1557/mrs.2019.104](https://doi.org/10.1557/mrs.2019.104). URL: <http://link.springer.com/10.1557/mrs.2019.104>.
- [22] C. A. Dennett and M. P. Short, “Thermal diffusivity determination using heterodyne phase insensitive transient grating spectroscopy,” *Journal of Applied Physics*, vol. 123, no. 21, p. 215109, Jun. 2018, ISSN: 10897550. DOI: [10.1063/1.5026429/15213310/215109__1__ACCEPTED__MANUSCRIPT.PDF](https://doi.org/10.1063/1.5026429/15213310/215109__1__ACCEPTED__MANUSCRIPT.PDF). URL: [/aip/jap/article/123/21/215109/124238/Thermal-diffusivity-determination-using-heterodyne](https://aip.org/jap/article/123/21/215109/124238/Thermal-diffusivity-determination-using-heterodyne).
- [23] F. Hofmann, D. R. Mason, J. K. Eliason, A. A. Maznev, K. A. Nelson, and S. L. Dudarev, “Non-Contact Measurement of Thermal Diffusivity in Ion-Implanted Nuclear Materials OPEN,” 2015. DOI: [10.1038/srep16042](https://doi.org/10.1038/srep16042). URL: www.nature.com/scientificreports/.
- [24] A. Reza, H. Yu, K. Mizohata, and F. Hofmann, “Thermal diffusivity degradation and point defect density in self-ion implanted tungsten,” *Acta Materialia*, vol. 193, pp. 270–279, Jul. 2020, ISSN: 1359-6454. DOI: [10.1016/J.ACTAMAT.2020.03.034](https://doi.org/10.1016/J.ACTAMAT.2020.03.034).
- [25] R. E. Stoller, M. B. Toloczko, G. S. Was, A. G. Certain, S. Dwaraknath, and F. A. Garner, “On the use of SRIM for computing radiation damage exposure,” *Nuclear Instruments and Methods in Physics Research Section B: Beam Interactions with Materials and Atoms*, vol. 310, pp. 75–80, Sep. 2013, ISSN: 0168-583X. DOI: [10.1016/J.NIMB.2013.05.008](https://doi.org/10.1016/J.NIMB.2013.05.008).
- [26] C. Dennett, “In-situ investigation of the oxidation kinetics of Fe-12Cr-2Si using time-resolved transient grating spectroscopy,” Ph.D. dissertation, MIT, Cambridge, MA, Jun. 2017.

- [27] I. Ipatova, R. W. Harrison, S. E. Donnelly, M. J. Rushton, S. C. Middleburgh, and E. Jimenez-Melero, “Void evolution in tungsten and tungsten-5wt.% tantalum under in-situ proton irradiation at 800 and 1000°C,” *Journal of Nuclear Materials*, vol. 526, 2019, ISSN: 00223115. DOI: [10.1016/j.jnucmat.2019.07.030](https://doi.org/10.1016/j.jnucmat.2019.07.030).
- [28] M. Akiyoshi, L. M. Garrison, J. W. Geringer, H. Wang, A. Hasegawa, S. Nogami, and Y. Katoh, “Thermal diffusivity of irradiated tungsten and tungsten-rhenium alloys,” *Journal of Nuclear Materials*, vol. 543, p. 152594, Jan. 2021, ISSN: 0022-3115. DOI: [10.1016/J.JNUCMAT.2020.152594](https://doi.org/10.1016/J.JNUCMAT.2020.152594).
- [29] D. E. Armstrong, X. Yi, E. A. Marquis, and S. G. Roberts, “Hardening of self ion implanted tungsten and tungsten 5-wt% rhenium,” *Journal of Nuclear Materials*, vol. 432, no. 1-3, pp. 428–436, Jan. 2013, ISSN: 0022-3115. DOI: [10.1016/J.JNUCMAT.2012.07.044](https://doi.org/10.1016/J.JNUCMAT.2012.07.044).
- [30] R. A. Pitts, S. Carpentier, F. Escourbiac, *et al.*, “A full tungsten divertor for ITER: Physics issues and design status,” *Journal of Nuclear Materials*, vol. 438, no. SUPPL, 2013, ISSN: 00223115. DOI: [10.1016/j.jnucmat.2013.01.008](https://doi.org/10.1016/j.jnucmat.2013.01.008).
- [31] A. Danagoulian, J. N. Miske, and E. A. Klein, “Grasshopper, a Geant4 Front End: Validation and Benchmarking,” *2021 IEEE Nuclear Science Symposium and Medical Imaging Conference Record, NSS/MIC 2021 and 28th International Symposium on Room-Temperature Semiconductor Detectors, RTSD 2022*, 2021. DOI: [10.1109/NSS-MIC44867.2021.9875720](https://doi.org/10.1109/NSS-MIC44867.2021.9875720).
- [32] T. Hirai, S. Panayotis, V. Barabash, *et al.*, “Use of tungsten material for the ITER divertor,” *Nuclear Materials and Energy*, vol. 9, pp. 616–622, Dec. 2016, ISSN: 2352-1791. DOI: [10.1016/J.NME.2016.07.003](https://doi.org/10.1016/J.NME.2016.07.003).